CHAPTER

8

Doppler Phenomenology and Data Acquisition

William A. Holm, Mark A. Richards

Chapter Outline

8.1 INTRODUCTION

Many signal processing techniques used by modern radars take advantage of the differences in the Doppler frequency characteristics of targets, clutter, and noise to minimize the interference competing with the target signals, and thus to improve the probability of detection and the measurement accuracy. Consequently, it is useful to study the Doppler frequency characteristics of typical radar signals.

The chapter begins by showing how the Doppler shift predicted by special relativity reduces to the very good standard approximation commonly used in radar, including in this book. The dependence on radial velocity is described. The principal focus of this chapter is on the Doppler spectrum of pulsed radar signals. The spectrum of the received signal for idealized stationary and moving point targets viewed with a finite pulse train waveform is developed step by step with key Fourier transform relationships introduced as required. These results are used to illustrate the concept of Doppler resolution. Attention then shifts to practical measurement of Doppler shift using finite pulse trains and Fourier analysis of the pulse-to-pulse phase shift. In doing so, the idea of coherent detection, first introduced in Chapter 1, is revisited.

Finally, the contributions of noise, clutter, and moving targets are described to build an understanding of the range-Doppler or range-velocity distribution as viewed by stationary

or moving (airborne or spaceborne) radars. The clutter foldover (ambiguity) effects on this distribution of range and velocity ambiguities are described and illustrated.

8.2 DOPPLER SHIFT

If a radar and scatterer are not at rest with respect to one another, the frequency, f_r, of the received echo will differ from the transmitted frequency, f, due to the Doppler effect. A proper description of the Doppler shift for electromagnetic waves requires the theory of special relativity. Consider a monostatic radar, where the transmitter and receiver are at the same location and do not move with respect to one another. Suppose a scatterer in the radar field of view is moving with a velocity component, v, toward the radar. The theory of special relativity predicts that the received frequency will be [1,2]

$$f_r = \left(\frac{1 + v/c}{1 - v/c}\right) f \tag{8.1}$$

Thus, an approaching target causes an increase in the received frequency. Substituting $-v$ for v shows that a receding target decreases the received frequency. This is in keeping with the common experience of passing train whistles or ambulance sirens. These Doppler shifts can be used to advantage in radar to detect echoes from moving targets in the presence of much stronger echoes from stationary clutter or to drastically improve cross-range resolution when there is relative rotation between a target scene and the radar. Uncompensated Doppler shifts can also have harmful effects, particularly a loss of detection sensitivity for some types of waveforms.

Equation (8.1) can be simplified without significant loss of precision because the velocity of actual radar targets is a small fraction of the speed of light, c. For example, the value of v/c for a supersonic aircraft traveling at Mach 2 (about 660 m/s) is only 2.2×10^{-6}. Expand the denominator of (8.1) in a binomial series:

$$\begin{aligned} f_r &= (1 + v/c)(1 - v/c)^{-1} f \\ &= (1 + v/c)[1 + (v/c) + (v/c)^2 + \ldots] f \\ &= [1 + 2(v/c) + 2(v/c)^2 + \ldots] f \end{aligned} \tag{8.2}$$

Discarding all second-order and higher terms in (v/c) leaves

$$f_r = [1 + 2\,(v/c)] f \tag{8.3}$$

The difference, f_d, between the transmitted and received frequencies is called the *Doppler frequency* or *Doppler shift*. For this case of an approaching target it is

$$f_d = \frac{2v}{c} f = \frac{2v}{\lambda} \tag{8.4}$$

where λ is the transmitted wavelength and positive values of v correspond to approaching targets.

Because the velocity of typical targets is so small compared with the speed of light, the numerical values of Doppler shift are small compared with the radar radiofrequencies (RFs). Table 8-1 gives the magnitude of the Doppler shift corresponding to a velocity of 1 meter per second, knot, or mile per hour at various typical RFs. The Mach 2 aircraft,

TABLE 8-1 ■ Doppler Shift as a Function of Velocity and Frequency

Radiofrequency f		Doppler Shift f_d (Hz)		
Band	Frequency (GHz)	1 m/s	1 knot	1 mph
L	1	6.67	3.43	2.98
S	3	20.0	10.3	8.94
C	5	33.3	17.1	14.9
X	10	66.7	34.3	29.8
K_u	16	107	54.9	47.7
K_a	35	233	120	104
W	95	633	326	283

observed with the L-band radar, would cause a Doppler shift of only 4.4 kHz in a 1 GHz carrier frequency.

For a monostatic radar, the Doppler shift is proportional to the relative velocity along the line of sight (LOS) between the radar and target, called the *radial velocity*. Consider the example of an aircraft flying at v m/s and illuminated by a stationary radar as shown in Figure 8-1. If the angle between the velocity vector of the aircraft and the radar LOS is ψ, the radial velocity component is $v \cdot \cos\psi$ m/s and the Doppler shift becomes

$$f_d = \frac{2v}{\lambda}\cos\psi \tag{8.5}$$

Note that a *crossing target*, which is a moving target viewed at $\psi = 90^\circ$, will have a Doppler shift of 0 Hz. Thus, the magnitude of the Doppler shift is maximum when the target is traveling directly toward or away from the radar ($\psi = 0$ or π radians). The Doppler shift is zero, regardless of the target velocity, when the target is crossing orthogonally to the radar boresight ($\psi = \pi/2$ radians).

It is important to note that the angle, ψ, in equation (8.5) is measured with respect to the velocity vector of the radar, not the pointing direction of the antenna. The angle of

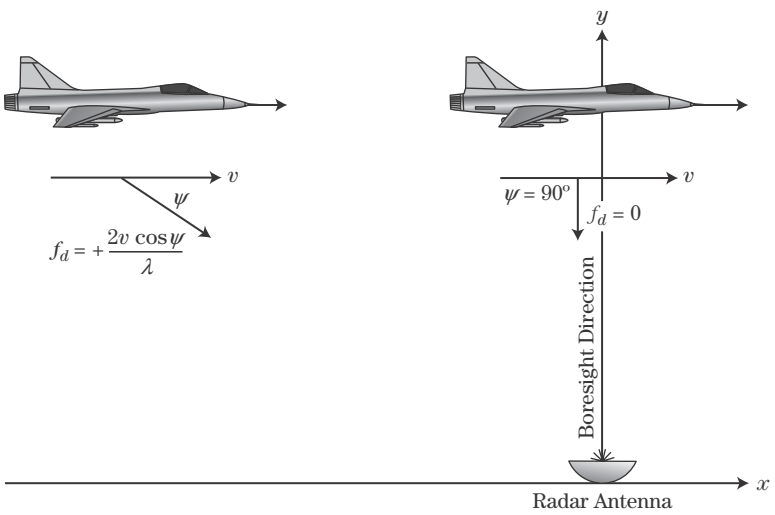

FIGURE 8-1 ■ Doppler shift is determined by the radial component of relative velocity between the target and radar.

the target with respect to the antenna determines the antenna gain in the target's direction, but not the Doppler shift of the echo. Also, note that the orientation of the aircraft body may differ from the velocity vector direction due to wind-induced crab, angle of attack, and similar effects.

8.3 THE FOURIER TRANSFORM

The frequency content of a time domain signal is analyzed by taking its Fourier transform, thus resulting in a frequency domain representation, or spectrum, of the time domain signal. Prior to discussing the Doppler frequency spectrum of radar signals, it is useful to briefly review the Fourier transform. Restricting consideration to continuous-time signals for the moment, if the time domain signal is described by the complex function $x(t)$, then its Fourier transform is given by

$$X(\omega) = \Im\{x(t)\} = \int_{-\infty}^{\infty} x(t)e^{-j\omega t}dt \tag{8.6}$$

where the operator $\Im\{\cdot\}$ represents Fourier transformation, and $j = \sqrt{-1}$. The frequency variable, ω, is in radians per second. It is related to the frequency, f, in hertz by the transformation $\omega = 2\pi f$. The Fourier transform can also be defined in terms of f as

$$X(f) = \Im\{x(t)\} = \int_{-\infty}^{\infty} x(t)e^{-j2\pi ft}dt \tag{8.7}$$

The time domain signal $x(t)$ can be regained by taking the inverse Fourier transform of $X(\omega)$ or $X(f)$:

$$x(t) = \frac{1}{2\pi}\int_{-\infty}^{\infty} X(\omega)e^{j\omega t}d\omega = \int_{-\infty}^{\infty} X(f)e^{j2\pi ft}df \tag{8.8}$$

Note that there is no factor of $1/2\pi$ on the inverse transform in terms of cyclical frequency f.

Consider an important but simple example, the infinite-length complex sinusoidal signal of amplitude A, $x(t) = A\exp(j2\pi f_0 t)$. Substituting this expression into equation (8.7) gives

$$\begin{aligned} X(f) &= \int_{-\infty}^{+\infty} (Ae^{+j2\pi f_0 t})e^{-j2\pi ft}dt = A\int_{-\infty}^{+\infty} e^{-j2\pi(f-f_0)t}dt \\ &= A\cdot\delta_D(f-f_0) \end{aligned} \tag{8.9}$$

where $\delta_D(f)$ is the *impulse* or *Dirac delta* function [3,4]. A plot of this spectrum is shown in Figure 8-2.

In the following, it is assumed that the reader is familiar with fundamental Fourier transform theorems and properties and with common Fourier transform pairs. The texts by Papoulis [3] and Bracewell [4] are excellent references for each of the properties and transform pairs used.

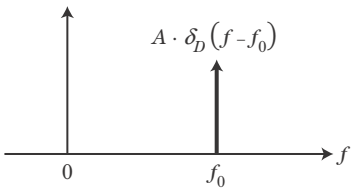

FIGURE 8-2 ■ Fourier transform of a complex sinusoid.

8.4 SPECTRUM OF A PULSED RADAR SIGNAL

It will be seen in Chapter 17 that Doppler processing relies on differences in Doppler shift between targets and interference, due to differences in velocity relative to the radar, to suppress the interference and allow target detection. For this reason, it is useful to consider the frequency spectrum of perhaps the most common radar waveform, a finite train of simple RF pulses, for both a stationary target and a moving target.

The finite RF pulse train radar signal can be described in terms of four increasingly long time scales: RF wave period, pulse width, pulse repetition interval (PRI), and coherent processing interval (CPI). The spectrum of the pulse train can be described in terms of four corresponding frequency scales: radar radiofrequency, pulse bandwidth, pulse repetition frequency (PRF), and spectral line bandwidth, respectively. A fundamental property of Fourier analysis is that the time and frequency scales have an inverse relationship to each other: the longer or more spread out a function is in time, the shorter or more compact is the corresponding frequency spectrum and vice versa. This *reciprocal spreading* relationship and its consequences are crucial to the understanding of Doppler processing techniques.

8.4.1 Spectrum of a Continuous Wave Signal

The simplest radar waveform is the real-valued infinite duration continuous wave (CW) sinusoidal signal of frequency f_0 Hz. It is defined by a single time scale, the period $T_0 = 1/f_0$. The spectrum consists of two impulse functions, one at f_0 and the other at $-f_0$. This can easily be seen by using the well-known Euler relation,

$$x(t) = A\cos(2\pi f_0 t) = \frac{A}{2}\left\{e^{j2\pi f_0 t} + e^{-j2\pi f_0 t}\right\} \tag{8.10}$$

and then taking the Fourier transform of $x(t)$ using equation (8.9) to get

$$X(f) = \frac{A}{2}[\delta_D(f - f_0) + \delta_D(f + f_0)] \tag{8.11}$$

Shown in Figure 8-3 is a plot of this waveform as a function of time and the resulting frequency-domain amplitude versus frequency plot.

Similarly, a sine function can be written by Euler's formula as

$$x(t) = \sin(2\pi f_0 t) = \frac{1}{2j}\{e^{j2\pi f_0 t} - e^{-j2\pi f_0 t}\} \tag{8.12}$$

and its Fourier transform as

$$X(f) = \frac{A}{2j}[\delta_D(f - f_0) - \delta_D(f + f_0)] \tag{8.13}$$

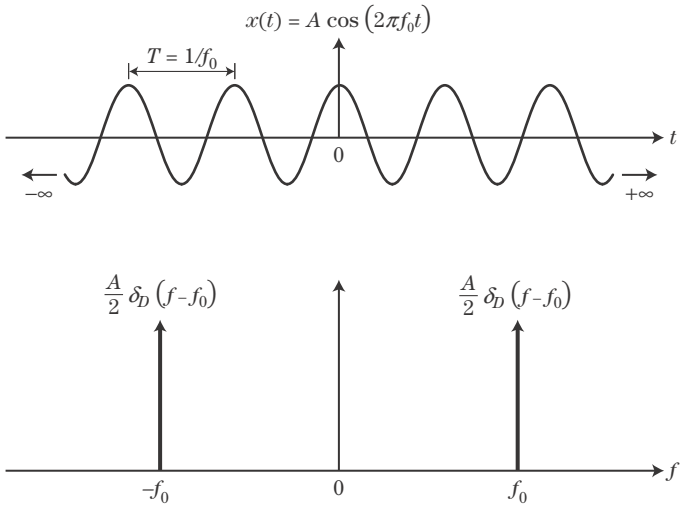

FIGURE 8-3 ■ Infinite-length continuous wave (CW) signal of frequency f_0 and its frequency spectrum.

8.4.2 Spectrum of a Single Rectangular Pulse

The spectrum of a finite-length series of modulated pulses is more complex but can be built up by a series of simple steps using the properties of Fourier transforms. Shown in Figure 8-4 is the time domain plot of a single pulse of pulse width, τ, and the magnitude of its corresponding spectrum. The waveform is defined using a single time scale parameter τ as

$$p_\tau(t) = \begin{cases} A, & -\frac{\tau}{2} \le t \le \frac{\tau}{2} \\ 0, & \text{otherwise} \end{cases} \tag{8.14}$$

Substituting this into equation (8.7), it is straightforward to show that

$$\begin{aligned} P_\tau(f) &= Ae^{-j2\pi ft}dt \int_{-\tau/2}^{+\tau/2} Ae^{-j2\pi ft}dt \\ &= \frac{A}{\pi f}\sin(\pi f\tau) = A\tau\frac{\sin(\pi f\tau)}{\pi f\tau} \\ &\equiv A\tau\,\mathrm{sinc}(\pi f\tau) \qquad \left(\mathrm{sinc}(z) \equiv \frac{\sin(\pi z)}{\pi z}\right) \end{aligned} \tag{8.15}$$

where the *sinc function*, which arises frequently in Fourier analysis, has been defined in the last step.

This spectrum has a $\sin f/f$ form centered at zero frequency. Notice that the nulls occur at integer multiples of $1/\tau$. The central portion of $X(f)$, between the frequencies $-1/\tau$ and $1/\tau$, is called the *main lobe* of the spectrum; the other lobes at frequencies outside of this range are called *sidelobes*. The width of the main lobe is characterized by one of several related metrics. The *Rayleigh width* is the width from the peak to the first null, which is $1/\tau$ Hz for this simple pulse. The *3 dB* or *half-power width* is the two-sided width measured at an amplitude corresponding to one-half the peak power, which occurs at $1/\sqrt{2}$ times the peak amplitude as shown in Figure 8-4. For the simple pulse, the 3 dB

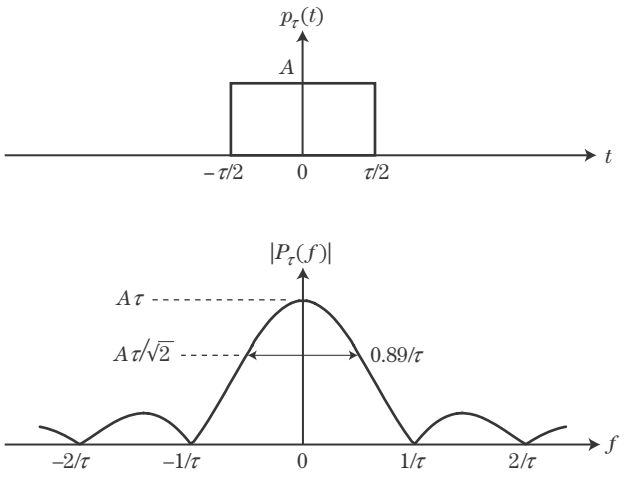

FIGURE 8-4 ■ A single simple pulse and its spectrum.

width is $0.89/\tau$ Hz.[1] Whichever metric is used, the width of the main lobe is inversely proportional to the pulse length. This is an example of the reciprocal spreading behavior of Fourier transforms previously mentioned.

8.4.3 Infinite Pulse Train

The second time scale is introduced by repeating the pulse at intervals of T seconds, creating an infinite pulse train. A convenient way to model the infinite pulse train is as the convolution of the single pulse, $p_\tau(t)$, of equation (8.14) with an infinite train of Dirac impulses spaced by the PRI of T seconds:

$$p_I(t) = \sum_{n=-\infty}^{\infty} p_\tau(t - n \cdot T) = p_\tau(t) \cdot \sum_{n=-\infty}^{\infty} \delta_D(t - n \cdot T) \tag{8.16}$$

Since $x(t)$ is the convolution of two terms, its Fourier transform is the product of the transforms of the two terms. The Fourier transform of an infinite pulse train in the time domain is another infinite pulse train in the frequency domain [4],

$$\Im\left(\sum_{n=-\infty}^{\infty} \delta_D\left(t - n \cdot T\right)\right) = \frac{1}{T}\sum_{k=-\infty}^{\infty} \delta_D\left(f - k \cdot \frac{1}{T}\right) = \frac{1}{T}\sum_{k=-\infty}^{\infty} \delta_D\left(f - k \cdot PRF\right) \tag{8.17}$$

The product of this spectrum with that of the single pulse in equation (8.15) is

$$P_I(f) = \{A\tau \operatorname{sinc}(\pi f \tau)\} \cdot \left\{\frac{1}{T}\sum_{k=-\infty}^{\infty} \delta_D\left(f - k \cdot PRF\right)\right\} \tag{8.18}$$

[1]Different bandwidth metrics are traditional in different technical specialties. While 3 dB metrics are common in radar, the Rayleigh bandwidth is common in optics. Other fields use the null-to-null bandwidth (twice the Rayleigh bandwidth). The "full width at half maximum" (FWHM), which is similar to the 3 dB width but measured at the 50% amplitude level, is common in spectroscopy.

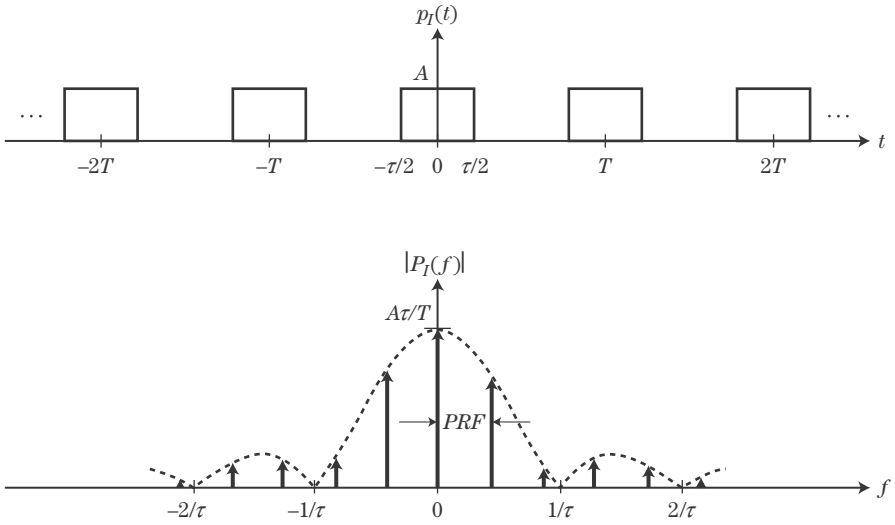

FIGURE 8-5 ■ Infinite pulse train signal and its spectrum.

The *sifting property* of impulses states that $X(f) \cdot \delta_D(f - f_0) = X(f_0) \cdot \delta_D(f - f_0)$; that is, the product of an impulse and a regular function is an impulse with a weight determined by the function. Applying this property to equation (8.18) shows that the spectrum of the infinite pulse train is an infinite series of spectral lines weighted by the spectrum of the single pulse. Specifically,

$$P_I(f) = \frac{A\tau}{T} \sum_{k=-\infty}^{\infty} \text{sinc}\,(\pi\tau k \cdot PRF) \cdot \delta_D\,(f - k \cdot PRF) \tag{8.19}$$

The time- and frequency-domain sketches of an infinite sequence of pulses are shown in Figure 8-5. The broad sinc term of the single pulse has been resolved into distinct spectral lines having zero bandwidth and separated by a frequency spacing equal to the PRF. In practice, the PRI varies from just a few times to perhaps 100 times the pulse length, so the number of spectral lines in one lobe of the broader sinc weight function ranges from a few, similar to the situation in Figure 8-6, to a very dense set of lines.

8.4.4 Finite Pulse Train

The third time scale is introduced by truncating the infinite pulse train to a finite series of pulses of total duration, T_d. T_d is called the *coherent processing interval*.[2] The finite pulse train waveform is modeled as the infinite pulse train of equation (8.16) multiplied by a simple pulse like that of equation (8.14), but with duration T_d (where $T_d > \tau$) and unit amplitude ($A = 1$):

$$p_F(t) = p_I(t) \cdot p_{T_d}(t), \quad p_{T_d}(t) = \begin{cases} 1, & -\dfrac{T_d}{2} \le t \le \dfrac{T_d}{2} \\ 0, & \text{otherwise} \end{cases} \tag{8.20}$$

[2]Recall that the term CPI is sometimes used interchangeably with *dwell time*. As discussed in Chapter 3, here dwell time is considered to be the amount of time a given target is within the antenna mainbeam on a single scan. There may be several CPIs in a dwell time.

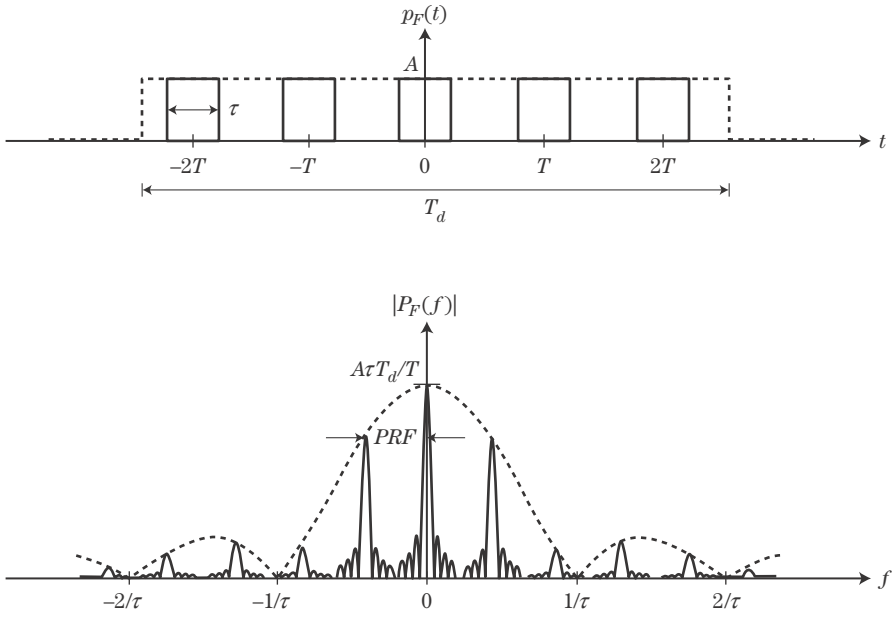

FIGURE 8-6 ■ Finite pulse train signal and its spectrum.

Since the waveform is the product of these two terms in the time domain, its Fourier transform is the convolution in frequency of the transforms of the two terms, which are given by equations (8.15) (with τ replaced by T_d and $A = 1$) and (8.19). Using the convolution property of impulses, $X(f) \cdot \delta_D(f - f_0) = X(f - f_0)$, the spectrum of the finite pulse train becomes

$$\begin{aligned} P_F(f) &= T_d \text{sinc}(\pi f T_d) \cdot P_F(f) \\ &= T_d \text{sinc}(\pi f T_d) \cdot \left\{ \frac{A\tau}{T} \sum_{k=-\infty}^{\infty} \text{sinc}(\pi \tau k \cdot PRF) \cdot \delta_D(f - k \cdot PRF) \right\} \\ &= \frac{AT_d\tau}{T} \sum_{k=-\infty}^{\infty} \text{sinc}(\pi \tau k \cdot PRF) \text{sinc}[\pi (f - k \cdot PRF) T_d] \end{aligned} \tag{8.21}$$

The resulting time-domain and frequency-domain plots are shown in Figure 8-6.

8.4.5 Modulated Finite Pulse Train

Finally, $p_F(t)$ is multiplied by a cosine function of frequency f_0 Hz to produce a finite train of modulated pulses:

$$x(t) = p_F(t) \cdot \cos(2\pi f_0 t) \tag{8.22}$$

The cosine function introduces the fourth time scale, the period $T_0 = 1/f_0$ of the modulating sinusoid.

The spectrum of the modulated pulse train can be determined using the modulation property of Fourier transforms, which states that if $x(t)$ has a Fourier transform $X(f)$, then

the transform of $x_m(t) = x(t)\exp(j2\pi f_0 t)$ is

$$\begin{aligned} X_m(f) &= \int_{-\infty}^{\infty} x(t)\, e^{j2\pi f_0 t}\, e^{-j2\pi f t} dt = \int_{-\infty}^{\infty} x(t)\, e^{-j2\pi (f - f_0)t} dt \\ &= X(f - f_0) \end{aligned} \tag{8.23}$$

That is, modulating a waveform by a complex exponential of frequency f_0 Hz merely shifts the waveform spectrum in frequency by f_0 Hz but does not change its shape. Applying this property along with Euler's formula to equation (8.21), the Fourier transform of the modulated pulse can be written immediately:

$$\begin{aligned} X(f) &= \frac{1}{2}\{P_F(f - f_0) + P_F(f + f_0)\} \\ &= \frac{AT_d\tau}{T}\left\{ \sum_{k=-\infty}^{\infty} \text{sinc}(\pi\tau k \cdot PRF)\text{sinc}[\pi(f - f_0 - k \cdot PRF)T_d] \right. \\ &\quad \left. + \sum_{k=-\infty}^{\infty} \text{sinc}(\pi\tau k \cdot PRF)\text{sinc}[\pi(f + f_0 - k \cdot PRF)T_d] \right\} \end{aligned} \tag{8.24}$$

The magnitude of $X(f)$ is plotted in Figure 8-7. It has the form of two sets of sinc-shaped spectral lines. The sets are centered at $f = \pm f_0$ and each is weighted by a broader sinc function. Each spectral line now becomes a narrow sinc function with Rayleigh bandwidth of $1/T_d$ Hz. Thus, four frequency scales are present in the description of the spectrum of a pulse waveform: (1) the bandwidth of the spectral lines $(1/T_d)$; (2) spacing of the spectral

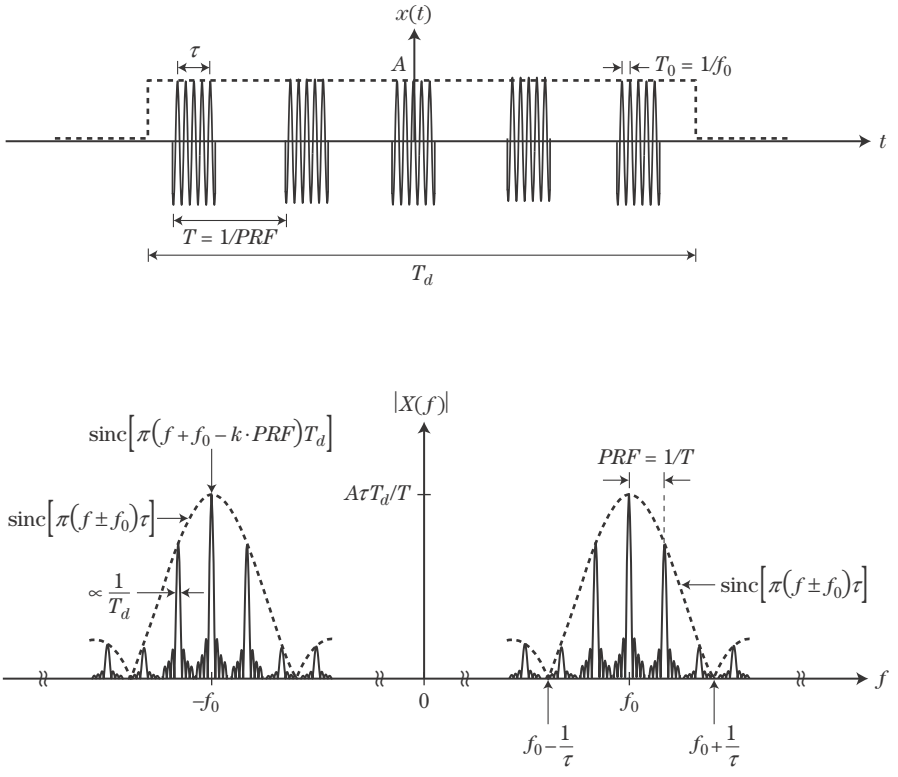

FIGURE 8-7 ■ Finite duration modulated pulse train signal and its Fourier transform.

lines ($PRF = 1/T$); (3) Rayleigh bandwidth of the single-pulse sinc envelopes ($1/\tau$); and (4) center frequencies of those envelopes ($\pm f_0 = \pm 1/T_0$). In practice, the intermediate frequency (IF) or RF f_0 would normally be from one to several orders of magnitude greater than the sinc weighting function Rayleigh width of $1/\tau$ Hz. For instance, a 1 μs pulse from a 1 GHZ radar would have $f_0 = 1$ GHz and $1/\tau = 1$ MHz, a difference of three orders of magnitude.

8.4.6 Pulsed Waveform Spectrum with Moving Targets

For a stationary radar, if the pulsed radar return is from a radar resolution cell that contains both a stationary target (clutter) and a moving target, then the return will consist of a superposition of signals. The signal from the stationary clutter will be at the transmitted RF f_0, and the signal from the moving target will be at $f_0 + f_d$, where $f_d = 2v/\lambda$ is the Doppler frequency shift, v is the radial component of the moving target's velocity, (i.e., the component along the line of sight between the radar and the target), and λ is the wavelength of the transmitted wave. The Doppler frequency shift is positive for approaching targets and negative for receding targets.

Because the effect of the moving target is simply to change the echo frequency to $f_0 + f_d$, the spectrum of the echo signal from a moving target alone (no clutter) measured with the finite pulse train waveform will be identical to that of equation (8.24) and Figure 8-7, with f_0 replaced by $f_0 + f_d$. Thus, the weighted line spectrum is simply shifted by f_d Hz. The total (moving target plus clutter) spectrum is then the superposition of the target and clutter spectra as shown in Figure 8-8. In this figure, the higher-amplitude line spectrum is due to the clutter, while the lower-amplitude, shifted spectrum is due to the moving target.

The basic *moving target indication* (MTI) approach inherent in Doppler processing techniques is now obvious. In the spectrum of the received signal, the moving targets and stationary clutter are separated. Thus, by applying appropriate filtering, the stronger stationary clutter can be removed (filtered) from the spectrum, leaving only the weaker signature of the moving target. This process is described in detail in Chapter 17.

8.4.7 Doppler Resolution

The Rayleigh main lobe width of an individual spectral line, $1/T_d$ Hz, determines the Doppler *resolution* of the finite pulse train. This is the minimum difference in Doppler shift between two targets producing equal-amplitude responses at which they can be reliably

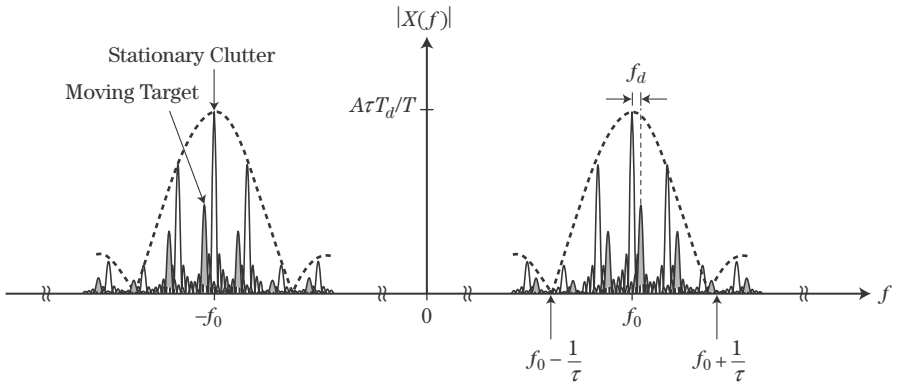

FIGURE 8-8 ■ Spectrum of the received signal from a moving target and stationary clutter.

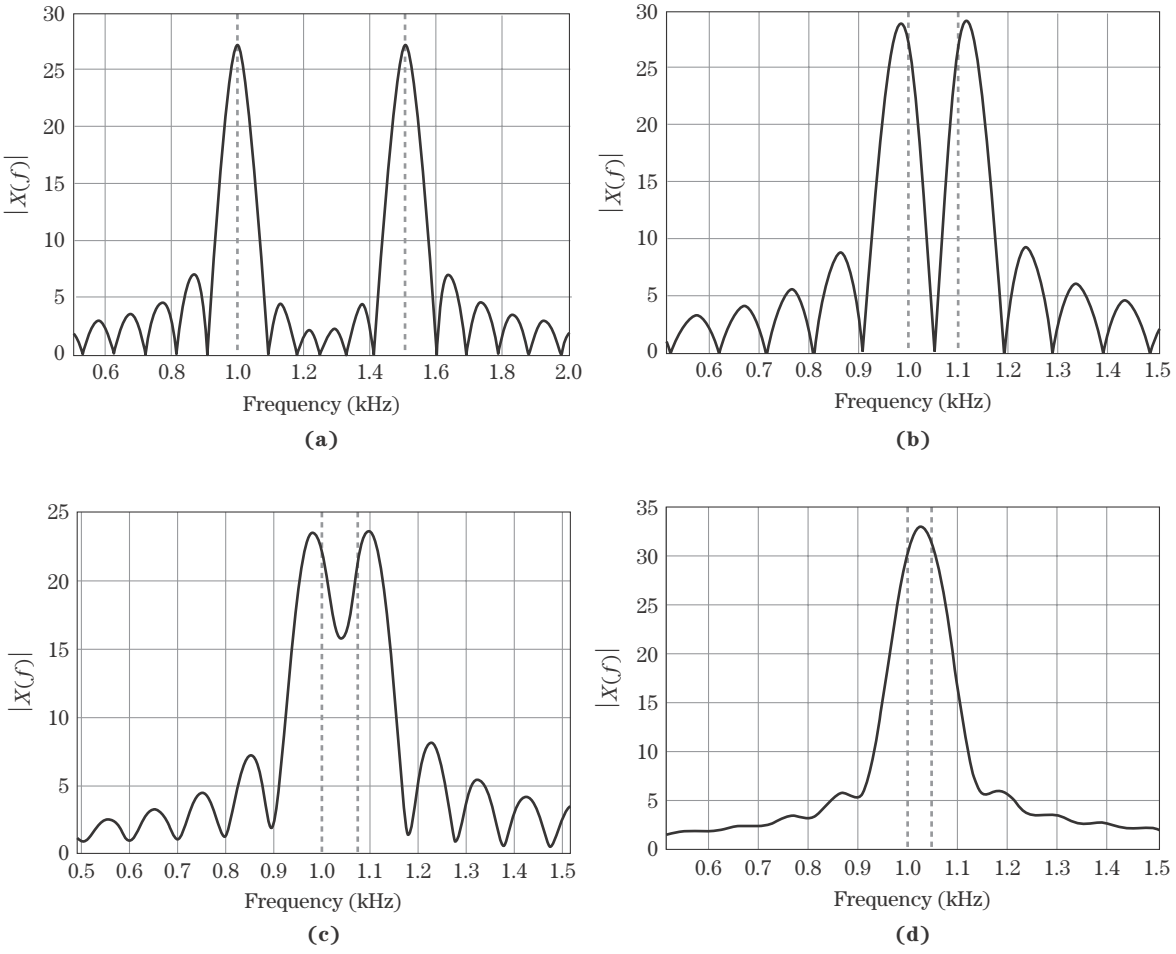

FIGURE 8-9 ■ Illustration of the concept of Doppler resolution. Individual spectral lines have 100 Hz Rayleigh bandwidth and zero relative phase. (a) 500 Hz spacing. (b) 100 Hz spacing. (c) 75 Hz spacing. (d) 50 Hz spacing.

distinguished from one another. The idea is illustrated in Figure 8-9. Part (a) of the figure shows a portion of the positive-frequency axis of the spectrum of two $T_d = 10$ ms pulse trains. A single spectral line of the spectrum from each is shown, one Doppler shifted to 1 kHz relative to the IF or RF and the other to 1.5 kHz. Because the pulse trains have a duration of 10 ms each, their individual spectral lines have Rayleigh (peak-to-first-null) bandwidths of 100 Hz. While the sidelobes of one spectrum affect the sidelobes and main lobe of the other, the two separate frequency components are obvious, and their peaks occur very close to the correct frequencies, which are marked by the vertical lines.

In the remaining parts of the figure, the pulse durations remain the same, but the spacing between their center frequencies are reduced to 100 Hz, then 75 Hz, then 50 Hz. At a spacing of 100 Hz, equal to the individual pulse Rayleigh bandwidth, there are still two easily recognizable distinct peaks. However, as the spacing is reduced to less than the pulse bandwidth, those peaks begin to blur together. When the spacing is 50 Hz, there is only a single peak, suggesting only a single-pulse frequency rather than two separate frequencies combined. While there is still some separation at 75 Hz spacing, there is

significant error in the peak locations, and the addition of noise to the signal would make it difficult to recognize the presence of two distinct peaks. Thus, the two different pulse frequencies are considered to be reliably separable, or *resolved*, when they are spaced by at least the single-pulse bandwidth, which in turn is determined by the CPI, T_d. The longer the pulse train, the finer the Doppler resolution.

The specific results of Figure 8-9 depend on the relative starting phase of the two sinusoids, which was zero in this example. Other choices of initial relative phase can make the frequency spacing at which the two signals are resolved smaller or larger. For example, a relative starting phase of 90° will result in two clearly distinct peaks in Figure 8-9d, although the peaks will be at about 960 and 1,090 Hz instead of the correct 1,000 and 1,050 Hz. On the other hand, a relative starting phase of 45° will cause the partial null between the peaks in Figure 8-9c to nearly disappear. The two peaks can be reliably resolved, regardless of initial relative phase, only if separated by approximately the Rayleigh resolution or more.

8.4.8 Receiver Bandwidth Effects

The modulated pulse train spectrum is not strictly band-limited; it has some energy out to $f = \pm\infty$. When the modulated pulse train reflects from a target and is received by the radar, the radar's receiver passband bandwidth will determine how much of the target signal energy is captured by the radar. As a starting point, the receiver bandwidth might be set to the reciprocal of the pulse length, $\pm 1/\tau$, centered at f_0, a total passband width of $2/\tau$ Hz. This choice is based on the bandwidth of the main lobe of the broader sinc function term of equation (8.24). It is sufficient to capture about 91% of the total energy in the broad sinc (i.e., 9% of the energy is in the sidelobes), only 0.43 dB less than the full energy of the sinc. The fraction of the total signal energy captured will depend on the density of the spectral lines within this sinc main lobe but will be similar to the 91% figure.

As the receiver bandwidth is increased, the amount of captured target energy increases, but only slightly. At most, only an additional 0.43 dB of signal power can be obtained by increasing the bandwidth. The amount of uniformly distributed (white) noise power at the receiver output, however, is proportional to the receiver bandwidth and therefore increases linearly as the bandwidth is increased. Depending on the level of the noise spectrum, there will be some point at which the noise level increases faster than the signal energy as the receiver passband is widened. Once this point is reached, the signal-to-noise ratio (SNR) at the receiver output will decrease with further increases in receiver passband width. On the other hand, if the bandwidth is reduced from a value of $2/\tau$, the output signal and noise powers are reduced at about the same rate. Therefore, the SNR is usually maximized when the receiver passband width is approximately $2/\tau$ Hz.

Another effect of reducing the receiver bandwidth is that the fidelity of the target signal is lost. Specifically, as the passband of the receiver is reduced below $f_0 \pm 1/\tau$ Hz, the effective width of the individual time domain pulses increases and the leading and trailing edges develop a more gradual slope, as depicted notionally in Figure 8-10. The degraded pulse echo shape has the effect of reducing the range resolution of the system (see Chapter 20) and the range tracking accuracy (Chapter 18). When using a simple pulse waveform, choosing the receiver bandwidth to be about $2/\tau$ Hz provides near-optimum SNR, resolution, and tracking accuracy. If the receiver filter frequency response is not a good approximation to an ideal rectangular response, the optimum bandwidth may be somewhat wider. In many cases the optimum bandwidth may be $2.4/\tau$ or $2.6/\tau$ Hz.

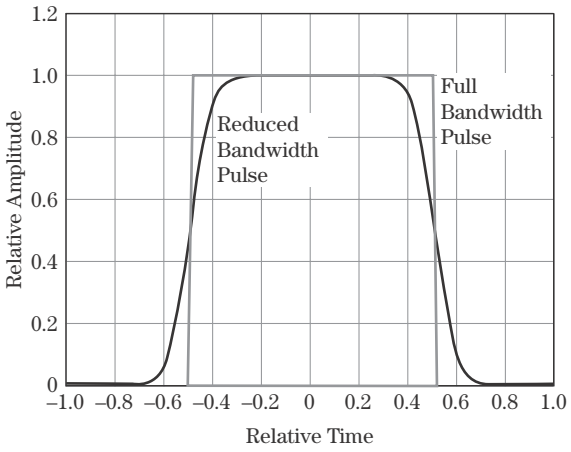

FIGURE 8-10 ■ Notional illustration of the effect of reduced bandwidth on pulse fidelity.

8.5 | WHY MULTIPLE PULSES?

Why is the spectrum of a series of pulses, rather than a single pulse, important in radar? One answer to this question can be had by considering typical values of Doppler shift. As an example, compute the number of cycles in a 10 μs X-band (10 GHz) pulse, with and without a rather high Mach 1 ($\sim$340 m/s = 22.7 kHz Doppler shift at X-band) Doppler shift. With no Doppler shift, the number of cycles is $(10^{10}$ cycles/sec$)(10^{-5}$ sec$) = 10^5 = 100{,}000$ cycles. With the Doppler shift, the number is $(10^{10} + 2.27 \times 10^4)(10^{-5}) = 100{,}000.227$ cycles, a change of only about one quarter of a cycle. It seems unlikely that such a small change in the waveform could be reliably measured. Put another way, 22.7 kHz Doppler shift is not resolvable in only 10 μs because the Doppler resolution is no better than 100 kHz, similar to the example of Figure 8-9 but with all frequencies higher by a factor of 1,000. The case described here would correspond to a frequency spacing of two signals that is only about half that of Figure 8-9d. If in addition one of the signals was weaker than the other and noise was present, the two signals could not be resolved.

This example is not contrived. In most radar systems, the bandwidth of a single pulse may be a few orders of magnitude greater than the expected Doppler frequency shift (i.e., $1/\tau \gg f_d$). Thus, the spectrum of the Doppler-shifted echo from a moving target is not significantly shifted from the spectrum of the stationary (and probably stronger) clutter echoes. Remembering that the frequency resolution in the Doppler process is proportional to the reciprocal of the waveform duration, the returns from many (often 20 or 30) consecutive pulses over a CPI $T_d \gg \tau$ must be analyzed in the frequency domain so that the single-pulse spectrum will separate into individual spectral lines with bandwidths approximately given by $1/T_d$. Then, as was implied in Figure 8-10, the Doppler frequency shift of the moving object is larger than the width of the individual spectral lines. The moving target spectral lines can then be separated from any stationary object returns.

In rare cases, the Doppler shift is greater than the single-pulse bandwidth, making it possible to measure Doppler shift with a single pulse. For example, a mach 20 target (6,700 m/s) detected at Ka-band (35 GHz) will have a Doppler frequency of about 1.6 MHz, which is significantly greater than the Doppler resolution of a 10 microsecond pulse. The resulting Doppler frequency will produce several (16) cycles of Doppler within a pulse, providing the ability to detect the target motion. However, this is unusual,

requiring a wide pulse, short wavelength, and very fast target. Since these conditions do not apply for most radar systems, only multiple pulse processing will be considered further.

An additional benefit of using multiple pulses for Doppler frequency estimation is that the required processing is a form of *coherent integration* that will improve target detection performance compared to a single-pulse measurement. Coherent integration and target detection are discussed in Chapter 15.

More realistic Doppler spectra are considered in Sections 8.8 and 8.9, but first it is necessary to discuss means for actually measuring Doppler shift in a modern radar system using a multiple pulse waveform. Before this can occur, however, the received signal must be detected. *Detection* in this sense means removal of the RF carrier frequency, a process also called *downconversion* or *demodulation*, to translate the echo signal energy to be centered at DC, where it is more easily processed. The downconverted signal is referred to as a *baseband* or *video* signal.

8.6 PULSED RADAR DATA ACQUISITION

8.6.1 Video Detectors and Phase Shift

Consider a single transmitted sinusoidal pulse at the radar's carrier frequency, f_0, centered at time $t = 0$:

$$\begin{aligned} x(t) &= A\cos(2\pi f_0 t + \theta), \quad -\frac{\tau}{2} \le t \le \frac{\tau}{2} \\ &= \mathrm{Re}\{Ae^{j(2\pi f_0 t+\theta)}\} = \mathrm{Re}\{(Ae^{j\theta})e^{j2\pi f_0 t}\}, \quad -\frac{\tau}{2} \le t \le \frac{\tau}{2} \end{aligned} \tag{8.25}$$

Assuming the RF frequency is known (as it normally would be), the pulse can be characterized by its amplitude A and phase θ, which together form the *complex amplitude* $Ae^{j\theta}$. Geometrically, the complex amplitude represents a vector of length A at an angle of θ with respect to the positive real axis in the complex plane. A coherent radar is designed to detect the rectangular components of the complex amplitude. Before discussing that process, however, it is useful to consider a single-channel detector.

Suppose the pulse of equation (8.25) reflects from a target at range, R_0. The received pulse will be

$$\begin{aligned} y_{\mathrm{I}}(t) &= x\left(t - \frac{2R_0}{c}\right) \\ &= A'\cos\left[2\pi f_0\left(t - \frac{2R_0}{c}\right) + \theta\right], \quad -\frac{\tau}{2} + \frac{2R_0}{c} \le t \le \frac{\tau}{2} + \frac{2R_0}{c} \\ &= A'\cos\left[2\pi f_0 t + \theta - \frac{4\pi}{\lambda}R_0\right], \quad -\frac{\tau}{2} + \frac{2R_0}{c} \le t \le \frac{\tau}{2} + \frac{2R_0}{c} \\ &= \mathrm{Re}\left\{A'\exp\left[j\left(\theta - \frac{4\pi}{\lambda}R_0\right)\right]\exp[j2\pi f_0 t]\right\}, \quad -\frac{\tau}{2} + \frac{2R_0}{c} \le t \le \frac{\tau}{2} + \frac{2R_0}{c} \end{aligned} \tag{8.26}$$

Compared with the envelope of the transmitted pulse, that of the received pulse has a new amplitude A' (modeled by the radar range equation) and is delayed in time by $2R_0/c$.

In addition to the delay of the pulse envelope, the phase of the received pulse is also shifted by $(-4\pi R_0/\lambda)$ radians. This phase shift, proportional to the range of the target, is

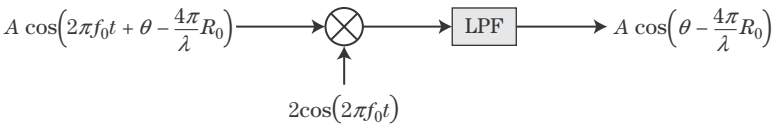

FIGURE 8-11 ■ Single-channel detector.

extremely important in coherent radar signal processing. For instance, a change in R_0 of $\lambda/4$ is sufficient to change the phase by π radians. Measuring phase changes thus provides a way to measure subwavelength range changes. This capability is the key to successful Doppler processing, adaptive interference cancellation, and radar imaging.

The goal of the radar is to measure the unknown parameters of the received pulse, namely, the amplitude A', time delay $t_0 = 2R_0/c$, and phase shift $\theta' = \theta - (4\pi/\lambda)R_0$. A block diagram of an idealized single-channel detector that achieves this is shown in Figure 8-11. The input is the sinusoidal pulse echo of equation (8.26). This signal is mixed with a reference oscillator at the RF. A simple trigonometric identity for the product of two cosine functions shows that, during the time that the input pulse is present, the signal at the output of the mixer consists of two terms, a sum frequency term $A'\cos[2\pi(2f_0)t + \theta']$ and a difference frequency term, $A'\cos\theta'$. The low-pass filter removes the sum frequency term so that the output is a sinusoidal pulse at a frequency of zero Hz, *i.e.* a constant pulse like that of Figure 8-4 with an amplitude of $A'\cos\theta'$. Note that this is just the real part of the complex amplitude $A'\exp(j\theta')$ of the received pulse. The voltage at the output of the detector is called the baseband or radar video signal. If the output of the detector is sampled at some time during the pulse, say at $t = 2R_0/c$, the measured value will be $y_I[0] = A'\cos\theta'$. The reason for the index [0] will be apparent shortly.[3]

8.6.2 Coherent Detector

The output voltage from the single channel detector of Figure 8-11 is not sufficient to identify both A' and the total phase. There are an infinite number of combinations of A' and θ' that will produce the same product $y_I[0]$. Furthermore, $\cos\theta' = \cos(-\theta')$, so the detector cannot distinguish between positive and negative phase shifts and therefore between positive and negative range changes.

This problem is solved by using the two-channel *coherent* or *I/Q detector* of Figure 8-12. This configuration splits the incoming signal into two channels. The upper channel signal is mixed with the reference oscillator $2\cos(2\pi f_0 t)$ as before, while the lower channel uses a reference oscillator of $2\sin(2\pi f_0 t)$. The lower oscillator is therefore 90° out of phase with the upper oscillator, a condition referred to as being *in quadrature* with respect to the upper channel. The upper channel is called the *in-phase* or *I channel* because it is the real part of the corresponding complex sinusoid; the lower is called the *quadrature* or *Q channel* and is the imaginary part of the complex sinusoid. A simple analysis of the Q channel similar to the previous example shows that its output voltage, when sampled at the appropriate time delay, is $y_Q[0] = A'\sin\theta'$ while the I channel output remains $y_I[0] = A'\cos\theta'$.

[3]The exact form of the result for $y[0]$ is valid under the "stop-and-hop" assumption, whereby it is assumed that the target movement while the pulse is in flight is negligible. This is an excellent approximation in most cases since the speed of propagation is much higher that target velocity. The stop-and-hop assumption is discussed in [5].

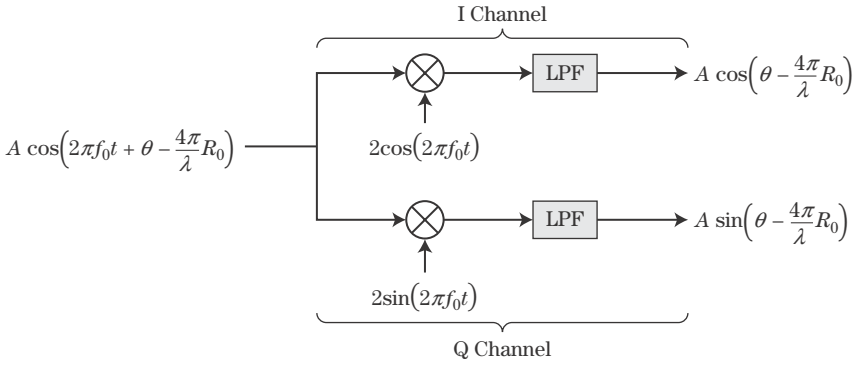

FIGURE 8-12 ■ Coherent or I/Q detector.

By itself, the Q channel does not resolve the ambiguities in measuring A' and θ'. However, a new, complex-valued signal y can be formed from the I and Q outputs:

$$\begin{aligned} y[0] &= y_{\mathrm{I}}[0] + j \cdot y_{\mathrm{Q}}[0] \\ &= A'(\cos\theta' + j\sin\theta') \\ &= A'\exp(j\theta') \end{aligned} \tag{8.27}$$

This complex output allows independent measurement of amplitude and phase. Specifically, $A' = |y[0]|$ and $\theta' = \tan^{-1}\theta'$.[4]

Repeating the coherent detection process for multiple samples forms a complex discrete-time signal $y[m] = y_{\mathrm{I}}[m] + j \cdot y_{\mathrm{Q}}[m]$ called the *analytic signal* [4]. The Q signal $y_{\mathrm{Q}}[m]$ is the negative of the Hilbert transform of the I signal $y_{\mathrm{I}}[m]$.

The diagrams in Figures 8-11 and 8-12 are useful models of the radar receiver and detector, but real receivers are more complex. In particular, downconversion is usually not performed with a single demodulation, but in two or more steps. The first steps translate the signal from RF to one or more IFs, while the last step translates that result to baseband. Chapter 11 discusses practical receiver architectures, and Chapter 10 describes the corresponding transmitter architectures to generate the radar signals. Chapter 11 also describes alternative receiver structures that derive the I and Q signals digitally from a single analog channel, a process often called *digital I/Q* or *digital IF* processing.

8.6.3 Range Bins

Use of the complex detector allows measurement of the received signal amplitude and phase. The time delay, t_0, is estimated by sampling the receiver output repeatedly after a pulse is transmitted and observing the time at which the echo is received. Time samples are generally taken at a spacing no greater than the time resolution of the radar pulse. For a basic pulse, this is simply the pulse length, τ. Thus, the receiver output is sampled every τ seconds from some initial time, t_1, to some final time, t_2. Since the echo received from a single scatterer is also τ seconds long, the echo will be present and contribute to only one time sample, say, at t'. Assuming the signal is strong enough to be detected, the time

[4]Care must be taken with the arctangent to place the result in the correct quadrant by taking into account the signs of y_{I} and y_{Q}.

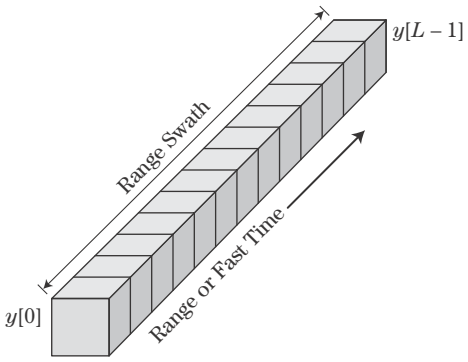

FIGURE 8-13 ■ Range bins and range swath. Each cube represents a single complex voltage measurement.

delay to the scatterer is estimated to be t' seconds, and the corresponding range estimate is $R' = ct'/2$ meters.

For the modulated pulses used for pulse compression (see Chapter 20), the sample spacing is generally is $1/B$ seconds, where B is the bandwidth of the pulse, corresponding to the compressed resolution of $c/2B$ m. Before pulse compression, the echo from a single pulse is spread out over $B\tau$ seconds. After pulse compression, the main lobe of the compressed response is limited to a single sample. (This is increased to typically 1.5 to 2 samples if windowing is used for sidelobe reduction.)

For each time sample, whether a received pulse is present, the output of the receiver will be sampled and a complex voltage, y, formed from the I and Q channel samples. This series of complex voltage measurements is typically stored in a computer memory as a one-dimensional vector as shown in Figure 8-13. The vector of samples is referred to by several names, including *range bins*, *range gates*, *range cells*, and *fast-time samples*. The interval from the range corresponding to the first sample to that corresponding to the last, that is, from $R_1 = ct_1/2$ to $R_2 = ct_2/2$ is called the range *swath*. Radars may have from as few as one to as many as several thousand range bins. The number of range bins can vary significantly in a single radar as it operates in different modes.

8.6.4 Pulsed Radar Data Matrix and Datacube

When the radar transmits M pulses in a dwell or CPI, a set of range gates like those of Figure 8-13 will be measured for each pulse. These are typically stored in memory as a two-dimensional matrix of complex voltage samples as shown in Figure 8-14a. The interval between samples in a row is the PRI, so the sampling rate in this dimension is the PRF. Because the PRF is much lower than the sampling rate in range, the pulse number axis is also called the *slow-time* dimension. Each row of the matrix represents a series of measurements from the same range bin over M successive pulses. The total amount of time MT represented by the data matrix is the dwell time or CPI.

Some radars operate multiple receivers simultaneously. Examples include phased array radars where the antenna is divided into subarrays, each with its own receiver. Another is a monopulse radar, where the antenna has three output channels (i.e., sum, azimuth difference, elevation difference), each with its own receiver. Each receiver will generate its own fast-time/slow-time data matrix for each CPI. It is common to represent the complete set of data by stacking these matrices into a *datacube* as shown in Figure 8-14b. The vertical axis is often called the receiver channel or *phase center* axis.

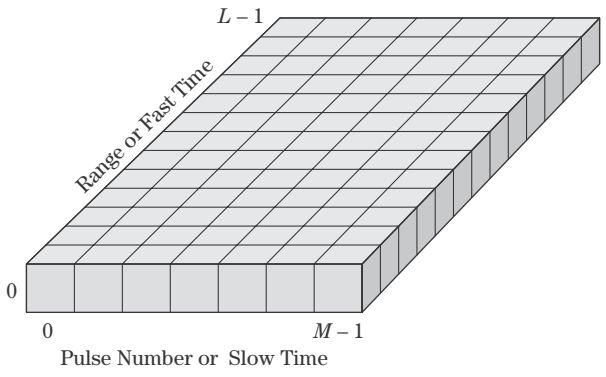

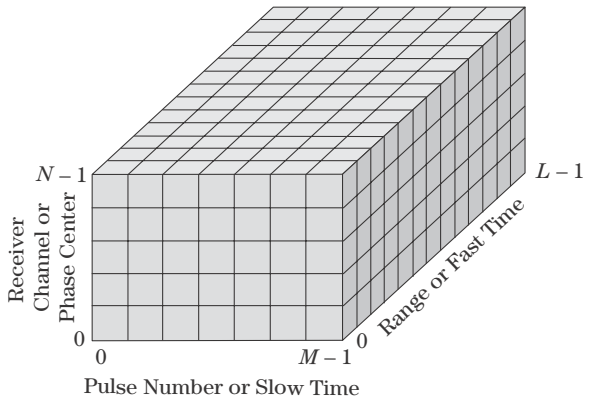

FIGURE 8-14 ■ (a) Fast-time/slow-time CPI data matrix. (b) Datacube.

8.7 DOPPLER SIGNAL MODEL

8.7.1 Measuring Doppler with Multiple Pulses

Now suppose the same target considered in the last section is approaching the radar with a radial velocity, v, and the radar transmits a series of M pulses separated by a PRI of T seconds. The range to the target when the m-th pulse ($0 \le m \le M-1$) is transmitted is $R_0 - mvT$ meters. The phase shift of the echo of the m-th pulse, following exactly the same argument as before, will be $(-4\pi/\lambda)(R_0 - vmT)$ radians. When the coherent detector output is sampled sometime during the echo (e.g., at $t = 2R_0 + mT$), the measured output for the m-th pulse will be

$$\begin{aligned} y[m] &= A\exp\{j[\theta - (4\pi/\lambda)(R_0 - vmT)]\} \\ &= A\exp\left\{j\left[2\pi\left(\frac{2v}{\lambda}\right)(mT) + \theta - \left(\frac{4\pi R_0}{\lambda}\right)\right]\right\} \\ &= A\exp[j(2\pi f_d t_m + \theta')], \quad 0 \le m \le M-1 \end{aligned} \tag{8.28}$$

where $t_m = mT$ is the transmit time for the m-th pulse. Equation (8.28) shows that the sampled signal formed by measuring the phase of each successive pulse echo with a multi-pulse waveform forms a discrete-time complex sinusoid at the expected Doppler

frequency! The signal is sampled at times t_m separated by the PRI. The sinusoid is the result of the changing echo phases, which in turn are caused by the changes in target range between pulses. Doppler shift measured from a series of phase measurements in this way is sometimes referred to as *spatial Doppler*.

The PRI is greater than the pulse length, sometimes by a large factor. In addition, the measurement is made with multiple (usually in the low tens, but sometimes much more) pulses. The resulting total observation time (CPI) of $T_d = MT$ seconds is typically an order of magnitude or more longer than a single pulse, giving a Doppler resolution of $1/MT$ Hz that is at least an order of magnitude finer than the $1/\tau$ Hz resolution of a single pulse. By choosing the CPI appropriately, it is possible to measure Doppler shifts on the scale needed in radar. For example, 20 pulses at a moderate PRF of 5 kHz gives a Doppler resolution of 250 Hz. Referring back to Table 8-1, this is a velocity resolution of 37 m/s (84 mph) in a 1 GHZ radar, and 3.7 m/s (8.4 mph) in a 10 GHz radar; recall that the single-pulse X-band measurement in Section 8.5 could not resolve even a Mach 1 Doppler shift. With the moving targets and clutter resolved in frequency, the detector output can now be filtered to separate moving targets from stationary targets. Moving target indication and pulse-Doppler processing techniques to do this are discussed in Chapter 17.

A common concern in measuring Doppler with finite pulse trains is that a moving target will move from one range bin to another over the course of a CPI, so its echo will not be present in all the pulses for a given range bin and equation (8.28) may not apply. That is, the target may not stay in one range bin over the entire CPI. For the velocities and CPI durations involved in Doppler processing, this *range migration* is rarely an issue. Consider a radar with relatively good 100 Hz Doppler resolution. The CPI is therefore a relatively long $1/100$ Hz $= 10$ ms. A typical pulse length in this scenario is at least $\tau = 1$ μs, so that the range bin spacing will be at least $c\tau/2 = 150$ m. An aircraft closing on the radar at a high velocity of Mach 2 (about 680 m/s) travels only 6.8 m during the CPI. Since this is much less than a range bin, it is generally safe to assume the target stays in the same range bin for the entire CPI and that equation (8.28) is a valid model. On the other hand, in Chapter 21 it will seen that range migration is very common in imaging radars due to a combination of much shorter range bins with much longer CPIs.

8.7.2 Coherent Pulses

To measure Doppler shift using multiple pulses, a deterministic phase relationship from pulse to pulse must be maintained over the CPI so that phase shifts measured by the coherent radar are due to relative radar-target motion only. Pulse trains that have this quality are called *coherent* pulse trains, and radars that can generate coherent pulse trains and measure the phase of the echoes are called coherent radars.

Figure 8-15 shows two pulse pairs—one coherent and one not. The center waveform is the output of a very stable oscillator. It provides a constantly running reference frequency for the receiver (as well as for the transmitter). The two upper pulses are both, when they are "on," in phase with this reference oscillator. Mathematically, they both have exactly the same sinusoidal formula; only the position of the rectangular pulse envelope $A(t)$ changes to turn the successive pulses on and off at different times t_1 and t_2, respectively.

This is not true of the two pulses at the bottom of the figure. The first pulse is the same as the first pulse of the coherent pair, and is in phase with the reference oscillator. The second pulse has the same frequency but is out of phase with the reference oscillator.

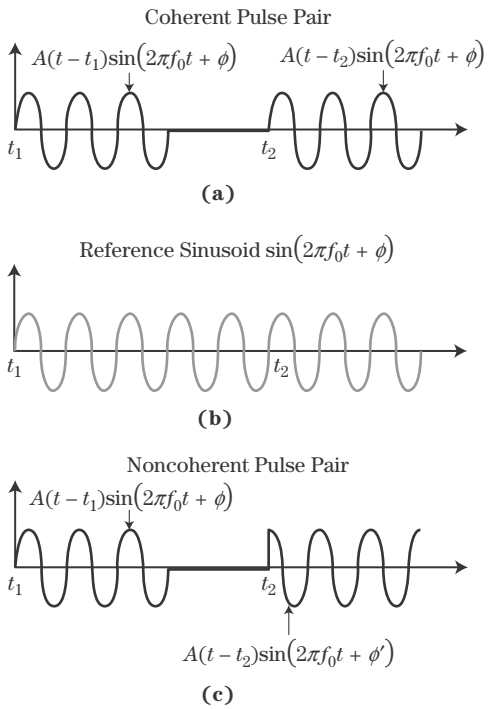

FIGURE 8-15 ■ (a) Coherent pulse pair. (b) Reference oscillator. (c) Noncoherent pulse pair.

Thus, the sinusoidal term of the second pulse formula is different. This pair of pulses would be considered *noncoherent*.[5]

Radar coherency is obtained by deriving the transmit RF signal from very stable oscillator sources that exhibit very little phase drift. The same oscillators are used in the transmit process and in the receiver downconversion or demodulation process. Any undesired phase shift in these oscillators will impart false phase modulations on the measured echo data. These errors often appear as a false Doppler signature on all objects, including stationary objects. Since phase drifts and phase noise build up over time, they can limit Doppler processing capability at longer ranges in some systems. Practical architectures for generating and receiving coherent radar signals are described in Chapters 10 and 11, respectively.

8.8 | RANGE-DOPPLER SPECTRUM FOR A STATIONARY RADAR

8.8.1 Elements of the Doppler Spectrum

The signal at the output of a real coherent radar detector is the superposition of some or all of the following components:

- Echoes from one or more moving or stationary targets.
- Receiver noise.

[5]If the actual phase of each pulse can be measured on transmit, then the phase difference can be compensated on receive, so coherent processing is possible. Radars that do this are called *coherent on receive* systems. It is preferable to make the system coherent to begin with.

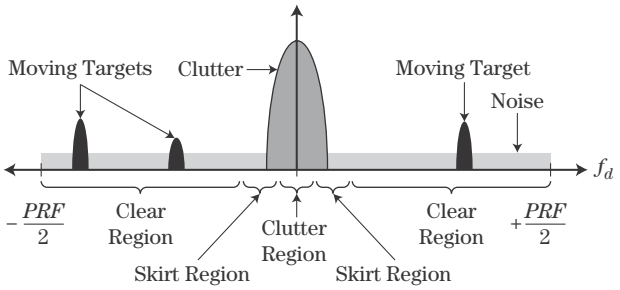

FIGURE 8-16 ■ Notional Doppler spectrum for one range bin, viewed by a stationary radar.

- Atmospheric and galactic noise.
- Spurious receiver mixer products.
- Echoes from clutter.
- Electronic countermeasures (ECM, also known as electronic attack [EA]) signals (jammers).
- Electromagnetic interference (EMI) signals, such as cell phones, other radars, or other services operating in the same or nearby frequency bands.

Not all of these are present in every case. In this chapter, attention is focused primarily on targets, clutter, and noise. Also, the radar itself may be stationary or moving (e.g., on an aircraft or satellite).

The Doppler spectrum for a range bin is the *discrete-time Fourier transform* (DTFT) of the slow-time data for that bin (see Chapter 14). Each of the aforementioned signal types will have different Doppler spectrum "signatures." The Doppler spectrum observed at the radar output will be the superposition of the contributions from each signal source.

Consider a stationary coherent radar first, and suppose its antenna is oriented such that it illuminates a scene where a particular range bin contains some ground clutter and three moving targets, one approaching the radar and two receding. A notional view of the Doppler spectrum might appear as in Figure 8-16. Only the portion of the spectrum between $\pm PRF/2$ is shown because the spectrum of the sampled data repeats periodically outside of this region. The energy around zero Doppler shift is echo from essentially stationary clutter, such as buildings, trees, and grass. As discussed in Chapter 5, real clutter has some Doppler spread that depends on the type of clutter and the weather conditions. In addition, clutter from air conditioning fans, automobile traffic, and other not-quite-stationary sources can spread the clutter spectrum.[6] The low-level energy spread uniformly across the spectrum is the white noise generated within the receiver.

Finally, the three "blips" of energy, two at negative Doppler and one at positive Doppler, represent the three moving targets. Their specific locations on the Doppler axis depend on their individual radial velocities with respect to the radar and their amplitudes relative to the noise are determined by their individual SNRs. If the target radial velocity, v, is in the interval $(-\lambda \cdot PRF/4, +\lambda \cdot PRF/4)$, then the Doppler shift will be between $(-PRF/2, +PRF/2)$ and the Doppler peaks will be indicative of the actual radial velocity.

[6]Radar platform motion can significantly spread the clutter spectrum as shown in Section 8.9, but the discussion is limited to stationary radar here.

The Doppler shift, f_d, of targets with a velocity outside this range will alias to an apparent Doppler of $f_d + k \cdot PRF$, where the integer k is chosen such that the result falls in the range $(-PRF/2, +PRF/2)$. Chapter 17 discusses resolution of these ambiguities. The amplitude of the clutter with respect to the noise floor is determined by the *clutter-to-noise ratio* (CNR). The CNR is computed using the radar range equation, but with the target RCS replaced by the total RCS of a clutter resolution cell as discussed in Section 2.13 and again in Section 5.1.

The portion of the Doppler spectrum that is free from clutter, so that noise is the dominant interference, is often called the *clear region*. This does not imply that targets at these Doppler shifts are clear of all interference, just of clutter. Noise is present at all Doppler shifts. The region of the spectrum where the clutter signal is stronger than the noise, so that clutter is the dominant interference, is called the *clutter region*. Sometimes a *skirt* or *transition region* is defined where the clutter and noise powers are approximately equal.

8.8.2 Range-Doppler Spectrum

Normally, there are many range bins. Targets may be present in several range bins, and the clutter will be distributed across many range bins. Furthermore, the clutter strength will vary with range, in part due to the fall-off in range due to the radar range equation and in part due to changes in the type of terrain producing the clutter at different ranges. Noise is present at all Doppler shifts and all ranges. Figure 8-17 is a notional illustration of the distribution of targets, clutter, and noise in both range and Doppler. The noise floor is constant through the range-Doppler space. The three targets are shown at approximately the same Doppler frequencies as in Figure 8-16 but are now in different range bins. Clutter is shown as the component centered on zero Doppler running through all of the range bins. The narrowing and lightening of the clutter ridge suggests the fall-off of the clutter power with range.

A range-velocity spectrum for a similar scenario using a 10 GHz radar, generated with a computer simulation, is shown in Figure 8-18. The left portion shows the distribution of power versus range and velocity in a three-dimensional format. The clutter ridge and

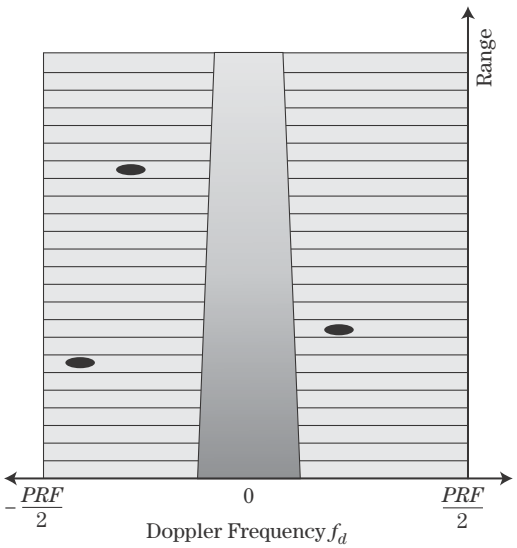

FIGURE 8-17 ■ Notional range-Doppler distribution viewed by a stationary radar.

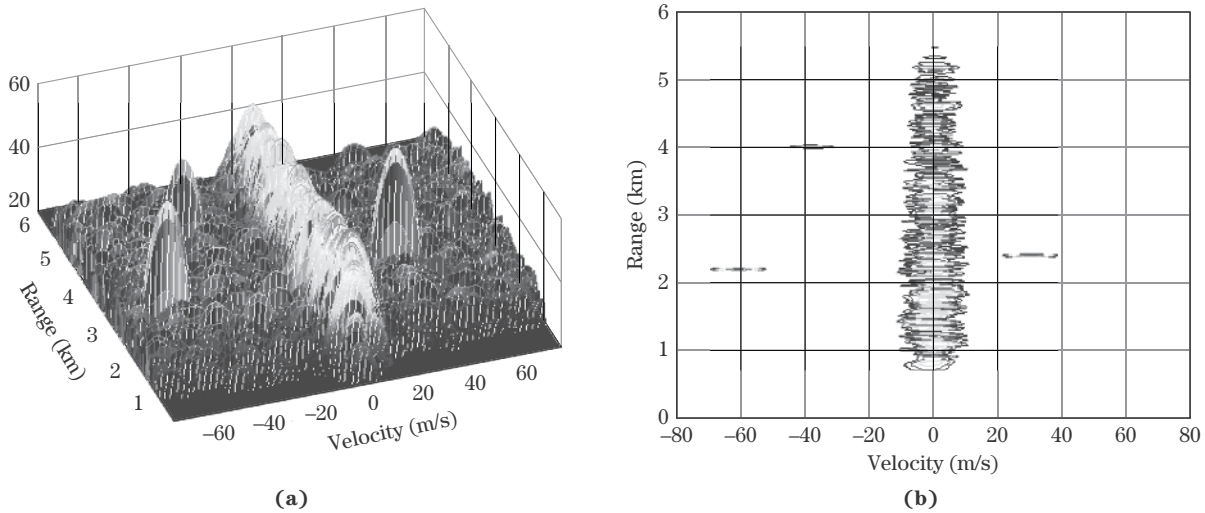

FIGURE 8-18 ■ Simulated range-Doppler distribution for a stationary radar with clutter and three moving targets. (a) Three-dimensional display. (b) Contour plot.

the three point targets are clearly visible above the noise floor. Part (b) of the figure shows the same data in a contour plot, with the lowest contour high enough to exclude the noise floor. (Figure 8-17 is essentially a stylized version of this contour plot.) This format makes it especially easy to visualize the target and clutter distribution.

The width of the point targets in Doppler is determined by the dwell time. A total of 30 pulses at a PRI of 100 μs were used, making the dwell time $T_d = 3$ ms. The Rayleigh resolution in Doppler is then $1/3$ ms $= 333$ Hz, corresponding to 5 m/s at 10 GHz, or 10 m/s null-to-null. The Doppler spectrum was computed with a Hamming window on the data to suppress Doppler sidelobes at the cost of doubling the Rayleigh bandwidth (see Chapter 14), so that the width of the peaks in Doppler is about 20 m/s, as can be seen in the figure.

8.9 | RANGE-DOPPLER SPECTRUM FOR A MOVING RADAR

8.9.1 Clutter Spreading

A moving radar not only adds a Doppler shift to the echo of stationary clutter according to equation (8.4), but it also induces a spread in the Doppler bandwidth of stationary clutter in the radar mainbeam. This is most relevant in air-to-ground radars. Figure 8-19 illustrates in two dimensions an approach to estimating the Doppler spread caused by radar platform motion. The 3 dB radar beamwidth is θ_3 radians. Recall that the Doppler shift for a radar moving at velocity v with its boresight squinted to a target ψ radians off the velocity vector is

$$f_d = \frac{2v}{\lambda} \cos \psi = f_{MLC} \text{ Hz} \tag{8.29}$$

Applied to stationary ground clutter observed from a moving platform, this formula describes the Doppler shift of the clutter on the radar boresight. The symbol f_{MLC} emphasizes that this is the Doppler shift of the main lobe clutter.

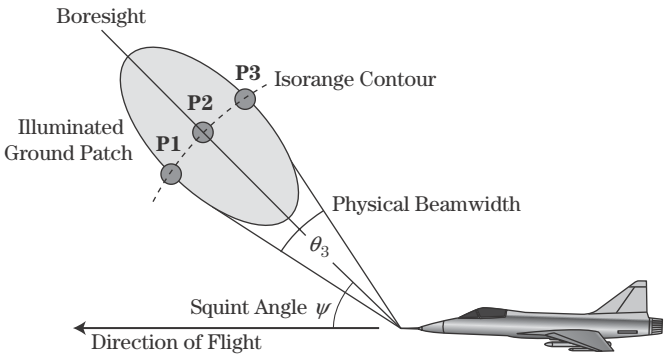

FIGURE 8-19 ■ Geometry for computing Doppler spread induced by radar platform motion.

Now consider three point scatterers **P1**, **P2**, and **P3**, each at the same range from the radar. **P1** and **P3** are at the 3 dB edges of the antenna beam, while **P2** is on boresight. Because all three are at the same range, the received echo at a delay corresponding to that range is the superposition of the echoes from all three scatterers. However, each is at a slightly different angle with respect to the aircraft velocity vector. **P2** is on the boresight at the squint angle of ψ, but **P1** and **P3** are at $\psi \pm \theta_3/2$ radians. The difference in the Doppler shift of the echoes from **P1** and **P3** is

$$\begin{aligned} B_{MLC} &= \frac{2v}{\lambda}\{\cos(\psi - \theta_3/2) - \cos(\psi + \theta_3/2)\} \\ &= \frac{4v}{\lambda}\sin\left(\frac{\theta_3}{2}\right)\sin\psi \end{aligned} \tag{8.30}$$

Radar antenna beamwidths are small, typically less than 5 degrees. Applying a small angle approximation to the $\sin(\theta_3/2)$ term in equation (8.30) gives a simple expression for the variation in Doppler shift of the main lobe clutter across the beam due to platform motion:

$$B_{MLC} \approx \frac{2v\theta_3}{\lambda}\sin\psi \text{ Hz} \tag{8.31}$$

The total Doppler bandwidth is approximately the sum of the bandwidth induced by platform motion and the intrinsic bandwidth of the scene being measured. Equation (8.31) assumes the radar is squinted sufficiently that the main beam does not include the velocity vector, that is, $|\psi| > \theta_3/2$. The formula must be modified if the main beam straddles the velocity vector.

As an example, an L-band (1 GHz) side-looking ($\psi = 90^\circ$) radar with a beamwidth of 3° traveling at 100 m/s will induce $B_d \approx 35$ Hz, while an X-band (10 GHz) side-looking radar with a 1° beam flying at 200 m/s will induce $B_{MLC} \approx 233$ Hz. This spreading of the clutter bandwidth can be either good or bad, depending on the radar's purpose. It complicates the detection of slow-moving surface targets from airborne platforms. On the other hand, this phenomenon provides the basis for obtaining cross-range resolution in imaging radars.

8.9.2 Clutter Spectrum Elements

The notional Doppler spectrum of Figure 8-16 can be greatly complicated by radar platform motion or Doppler ambiguities and by aliasing of the spectrum at low PRFs. Figure 8-20

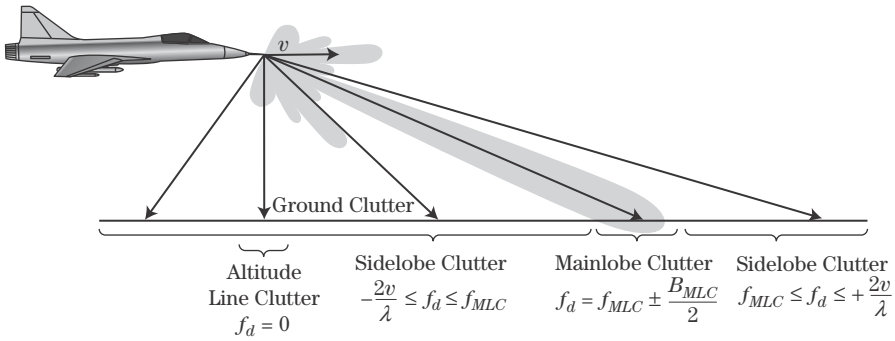

FIGURE 8-20 ■ Geometry for computing Doppler spread induced by radar platform motion.

is another view of a moving aircraft viewing stationary ground clutter, emphasizing that different patches of ground will provide echoes with different Doppler shifts due to different angles with respect to the velocity vector. In addition, these clutter echoes will have different strengths, depending on range and whether they are viewed through the antenna sidelobes or main lobe.

Figure 8-21 illustrates the resulting effects on the spectrum. For simplicity, all the signal components are shown in a single range bin's spectrum, though in reality, different components and targets will be in different range bins.

To begin, the entire Doppler spectrum is shifted by the nominal radar-to-ground Doppler shift of $f_{MLC} = 2v\cos\psi/\lambda$ Hz while the main lobe is widened by B_{MLC} Hz due to clutter spreading as described already. In addition to this broadened *main lobe clutter* (MLC), *sidelobe clutter* (SLC) and an *altitude line* (AL) are now evident as well. Sidelobe clutter results from energy radiated and received through the radar sidelobes. It is thus weaker than the main lobe clutter. Since sidelobes and backlobes exist in all directions, it is possible, depending on the aircraft direction, to receive echoes from ground or air clutter directly ahead of the aircraft as well as directly behind it. Any clutter present in these directions has a radial velocity equal to the full velocity, v, of the platform if in the direction of flight, or the negative of the velocity if behind the platform. Clutter at other angles creates echo energy at velocities between $+v$ and $-v$. Sidelobe clutter did not appear in the stationary radar case of Figure 8-16 because the sidelobe echoes occur at zero Doppler and are thus part of the main lobe clutter.

The altitude line results from the echo from energy transmitted through the sidelobes of an airborne radar straight down to the ground and back. The altitude line appears at the value of the radial velocity component toward the ground; in level flight this is zero, regardless of the platform velocity or antenna look direction. Although it is transmitted and received through the radar sidelobes, the altitude line nonetheless tends to be relatively strong due to the relatively short vertical range and the high reflectivity of most clutter at normal incidence. In a pulsed system, as will be seen shortly, the AL and MLC do not

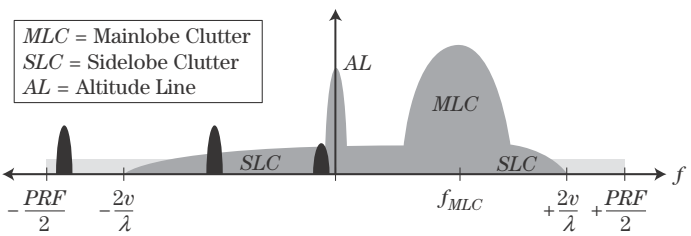

FIGURE 8-21 ■ Notional Doppler spectrum for moving radar platform (see text for details).

appear in the same range bin. The range to the altitude bounce is just the altitude of the platform, while the main lobe is usually steered to a longer range.

8.9.3 Range-Doppler Clutter Distribution

The spectrum of Figure 8-21 was used to introduce the major clutter components. However, clutter observed from a moving pulsed radar is distributed in complex patterns through the range-Doppler (equivalently, range-velocity) space. The total clutter power received in a given range-velocity cell is the sum of the power from all stationary clutter scatterers in the same range bin and having the same angle with respect to the platform velocity vector.

Since the Doppler shift of a stationary clutter scatterer is proportional to the cosine of the angle ψ between the velocity vector and the scatterer (often called the *cone angle* to the scatterer), all stationary scatterers located on a cone of half-angle ψ centered on the platform velocity vector will have the same Doppler shift. The intersection of a cone with a flat plane representing the ground is a conic section which can be either a hyperbola (if the radar travels parallel to the ground, i.e., level flight), a parabola (shallow dive), or ellipse (steep dive). Whatever its shape, this line is called an *isovelocity* or *isodoppler* contour (often *isodop* for short). Scatterers having the same range, *R,* from the radar are on the surface of sphere of radius, *R,* centered on the radar, which intercepts the ground plane on a circular locus called an *isorange* contour. Thus, scatterers at the intersection of a given isodop and isorange contour contribute power to the same range-Doppler cell.

Figure 8-22 is an example of circular isorange and hyperbolic isovelocity contours for a forward-looking radar traveling straight and level at 100 miles per hour at an altitude of 10,000 feet above the ground. Clutter scatterers at the two highlighted patches at a downrange coordinate of 68 km and cross-range of ± 75 km have the same total range of 100 km and velocity of 30 m/s relative to the radar and will therefore both contribute to the same range-velocity or range-Doppler cell.

Figure 8-23 shows a complete range-velocity clutter distribution for the same radar motion and geometry, taking into account the antenna gain and the variation of clutter reflectivity with grazing angle. A sinc-squared two-way antenna pattern with a Rayleigh beamwidth of 3.5° and minimum sidelobe level of -35 dB, and a constant-gamma clutter reflectivity were assumed. Part (a) of the figure gives a three-dimensional view, while part (b) displays the distribution in a plan view.

There are several notable features of the clutter distribution. There is no clutter return at all (only noise) until a range of approximately 3 km, corresponding to the 10,000 foot

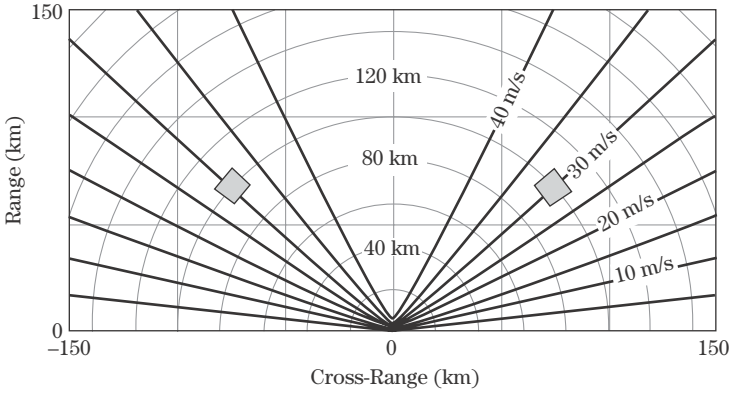

FIGURE 8-22 ■ Intersection of isorange and isovelocity contours.

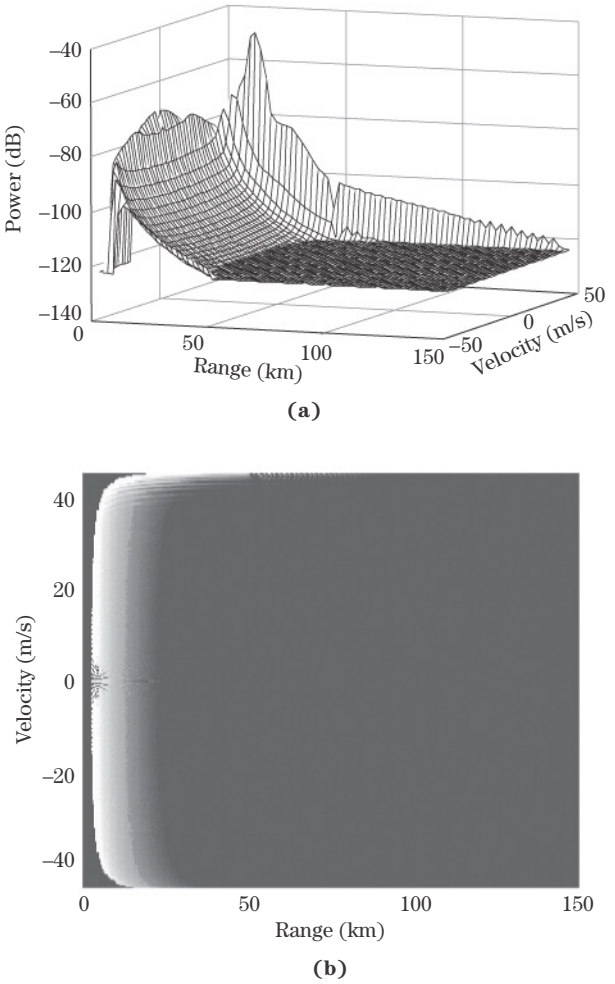

FIGURE 8-23 ■ Simulated range-velocity distribution for a stationary clutter observed from a moving radar (see text for details). (a) Three-dimensional display. (b) Plan view.

elevation of the aircraft. Note the relatively high clutter return strength at 3 km (the platform altitude) and zero velocity, which fades away rapidly as the range increases and the grazing angle decreases along the zero velocity line. This is the altitude line previously introduced; the high clutter return at short range and across all Doppler is called *near-in clutter*.

In this geometry, the boresight intercepts the ground at a range of just over 17 km and a grazing angle of only 10°. The strong peak at that range and a velocity nearly equal to the aircraft velocity is the main lobe clutter. Its greater amplitude is due to the main lobe antenna gain; the surrounding plateaus are due to the first few antenna sidelobes.

8.9.4 Range and Velocity Ambiguity Effects

The idea of a range ambiguity was introduced in Chapter 1. If the radar environment is such that the clutter echo from distances greater than the unambiguous range $R_{ua} = cT/2$ are significant, then clutter from longer ranges will "fold over" (alias) onto shorter ranges. This is more likely at higher PRFs (smaller T). Figure 8-24 illustrates this effect for a stationary radar at an altitude of 10,000 feet and a $-30°$ pointing angle, so that the boresight intercepts the ground at a range of about 5.3 km. The PRF is 20 kHz, giving

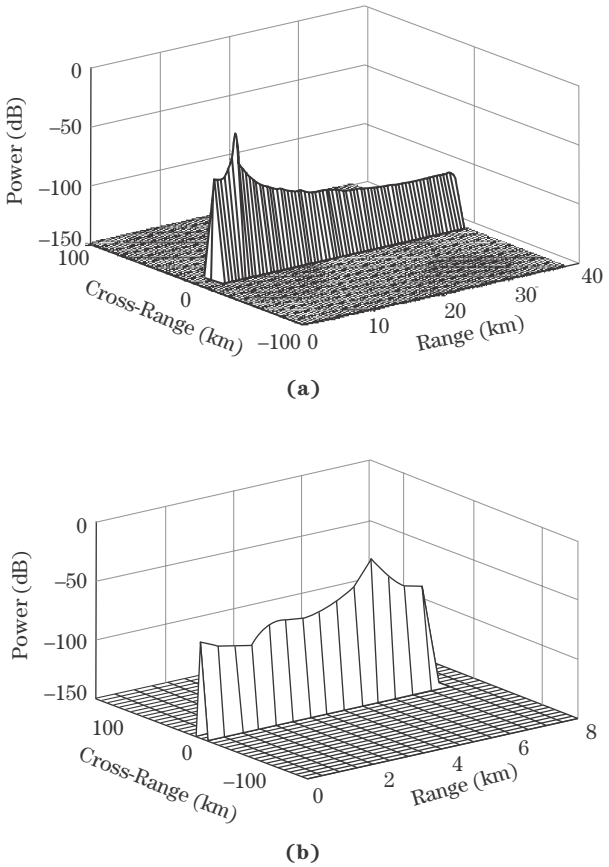

FIGURE 8-24 ■ Simulated range-velocity distribution for a stationary clutter observed from a stationary radar (see text for details). (a) Without clutter foldover. (b) With foldover.

an unambiguous range of 7.5 km. Figure 8-24a shows the actual distribution of clutter power versus range. The 3 km altitude, the main lobe peak at 5.3 km, and the fall-off in clutter power out to longer ranges are all evident. Figure 8-24b shows the clutter as would actually be measured by the radar. Note the change in range scales. Clutter in the intervals from, for example, 7.5 to 15 km and 15 to 22.5 "fold over" into the 0 to 7.5 km interval. While the main lobe peak is still apparent, the clutter power is generally flatter over range.

Ambiguities also occur in Doppler shift and thus in velocity. This is a consequence of Doppler being measured using the sampled slow-time data as was discussed in Section 8.6. The sampling rate in slow time is the PRF. The Nyquist sampling requirement (discussed in Chapter 14) limits the range of Doppler shifts that can be represented to $\pm PRF/2$, equivalent in velocity to $\pm v_{ua}/2$ where $v_{ua} = \lambda \cdot PRF/2$. If the platform velocity exceeds $v_{ua}/2$, then there will be clutter cells with Doppler shifts greater than $v_{ua}/2$. The echo from these cells will alias, wrapping around to a new value $v' = v + k \cdot v_{ua}$ for some integer k such that v' does fall within $\pm v_{ua}/2$. Velocity ambiguities are more likely to occur at low PRFs and high platform velocities.

Figure 8-25 is an example of the effect of velocity ambiguity on the range-velocity distribution of clutter. The conditions are the same as for Figure 8-23, except that the PRF has been lowered to 1 kHz. At the 10 GHz RF, this gives an unambiguous velocity of $v_{ua} = 15$ m/s, so the velocity range shown is ± 7.5 m/s. The clutter distribution is the same as in Figure 8-23b, except that now velocities greater than $+7.5$ m/s alias into

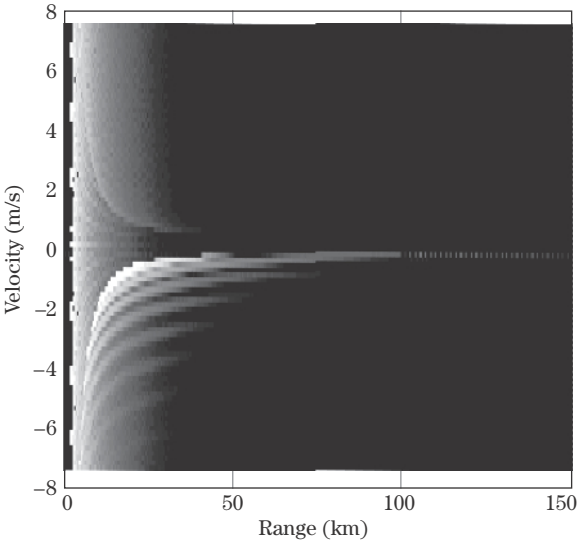

FIGURE 8-25 ■ Simulated range-velocity distribution for stationary clutter observed from a moving radar at low PRF. Compare to Figure 8-23b.

the interval ±7.5 m/s. For instance, the main lobe clutter, previously centered at about 17.3 km range and 44 m/s, still appears at 17.3 km range but now wraps around to $v' = 44 - 3 \cdot 15 = -1$ m/s.

In a so-called *medium PRF* radar, common in airborne systems, both range and velocity ambiguities may be present at the same time, resulting in complex distributions of clutter. Figure 8-26 is an example of the range-velocity clutter spectrum for an X-band radar traveling at 300 mph (134 m/s) with the antenna squinted 45° right in azimuth and 10° down. The main lobe is centered on the ground at a range of 17.3 km. The PRF is 20 kHz, giving an unambiguous range of 15 km and an unambiguous velocity interval of ±75 m/s. Thus, the clutter will fold over in both range and Doppler. To see this, notice the bright main lobe clutter signal. Although the radar is forward-looking so that the actual main lobe clutter Doppler is positive, it has folded over to a negative Doppler shift corresponding

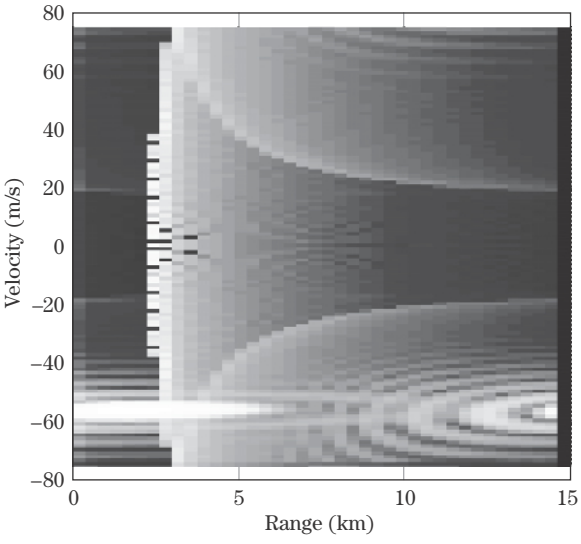

FIGURE 8-26 ■ Medium-PRF range-velocity clutter distribution (see text for details).

to about −58 m/s. The main lobe clutter is also wrapped in range: the peak occurs at the actual 17.3 km but folds over to 2.3 km. Furthermore, the main lobe peak is actually split across the 15 km unambiguous range.

As a final note, consider the area of the plot in Figure 8-26, which is a measure of the total range-velocity space in which targets and clutter can be located without encountering ambiguities. The product of R_{ua} and v_{ua} is

$$R_{ua}v_{ua} = \left(\frac{cT}{2}\right)\left(\frac{\lambda}{2}PRF\right) = \left(\frac{cT}{2}\right)\left(\frac{\lambda}{2T}\right) = \frac{\lambda c}{4} \tag{8.32}$$

which, for a given RF, is a constant. Thus, to increase the unambiguous range, the unambiguous velocity interval must be reduced and vice versa. In Chapter 17, *staggered PRF* techniques will be introduced as a way to expand the range-velocity coverage beyond the limit of equation (8.32).

8.10 FURTHER READING

Details of the measurement of Doppler shift using multiple pulses and discrete Fourier analysis and of the stop-and-hop approximation are given in the textbook by Richards [5]. More in-depth discussions and examples of the complexities of the range-Doppler or range-velocity distribution, especially for moving platforms, are found in the books by Morris and Harkness [6] and Stimson [7]. Stimson's book deserves special mention for its comprehensive, easy-to-understand discussion of airborne radar and its extraordinary illustrations. Schleher [8] provides an in-depth analytical discussion of Doppler signal characteristics.

8.11 REFERENCES

[1] Gill, T.P., *The Doppler Effect,* Logos Press, London, 1965.

[2] Temes, C.L., "Relativistic Consideration of Doppler Shift," *IRE Transactions on Aeronautical and Navigational Electronics*, p. 37, 1959.

[3] Papoulis, A., *The Fourier Integral and Its Applications*, 2d ed., McGraw-Hill, New York, 1987.

[4] Bracewell, R., *The Fourier Transform and Its Applications*, 3d ed., McGraw-Hill, New York, 1999.

[5] Richards, M.A., *Fundamentals of Radar Signal Processing*, McGraw-Hill, New York, 2005.

[6] Morris, G.V., and Harkness L. (Eds.), *Airborne Pulsed Doppler Radar*, 2d ed., Artech House, 1996.

[7] Stimson, G.W., *Introduction to Airborne Radar*, 2d ed., SciTech Publishing, Raleigh, NC, 2000.

[8] Schleher, D.C., *MTI and Pulsed Doppler Radar*, Artech House, Norwood, MA, 1999.

8.12 PROBLEMS

1. Consider a target approaching an L-band (1 GHz) radar at a radial velocity of 100 m/s. Estimate the error in the approximate formula for Doppler shift given by equation (8.4). (Note: the numerical precision required for this calculation may exceed that of many calculators. The

error can be estimated using tools such as MATLAB or Mathematica or by considering the terms neglected in the series expansion of (8.2).)

2. Suppose two aircraft are flying straight and level at the same altitude. One is traveling due north at 100 m/s, while the other is flying directly at the first but in the southwesterly direction, also at 100 m/s. What is the radial velocity between the two aircraft? What is the Doppler shift in hertz, including the sign, assuming an X-band (10 GHz) radar?
3. A stationary radar with a rotating antenna (typical of an airport approach radar, for instance) observes an aircraft moving through its airspace in a straight line at a speed of 200 mph. The aircraft approaches from the east, flies directly overhead of the radar at an altitude of 5 km, and continues to the west. Sketch the general behavior of the radial velocity of the target relative to the radar as it flies from east to west through the airspace. Label significant values.
4. Suppose a radar has a pulse length of 100 ns. What is the Rayleigh bandwidth of the pulse spectrum, in Hz? What is the 3 dB bandwidth in Hz?
5. Calculate the Rayleigh resolution in Doppler frequency corresponding to an RF pulse at a center frequency of 35 GHz and a pulse duration of 1 μs.
6. Consider two RF pulses at frequencies of 5.0 GHz and 5.01 GHz. What is the minimum pulse length required so that the two pulses could be reliably resolved in frequency (separated by one Rayleigh resolution)?
7. A finite pulse train waveform is composed of 20 pulses, each of 10 μs length and separated by a PRI of 1 ms. What is the coherent processing interval for this waveform? What is the peak-to-null Doppler resolution?
8. For the pulse train waveform of problem 7, sketch the spectrum in a form similar to Figure 8-6. Indicate the Rayleigh width and the spacing of the individual spectral lines. How many individual spectral lines fall within the main lobe of the sinc-shaped envelope determined by the pulse length?
9. Consider a simple pulse burst waveform with $M = 30$ pulses, each of 10 μs duration, and a PRI of $T = 100$ μs. Assuming no weighting functions are used, what are the range resolution, Doppler resolution, unambiguous range, and unambiguous Doppler shift associated with this waveform?
10. Consider a C-band (6 GHz) weather radar and suppose the desired velocity resolution is $\Delta v = 1$ m/s. What is the corresponding Doppler frequency resolution Δf required? If the PRF is 1,000 pulses per second, how many pulses, M, must be processed to obtain the desired velocity resolution, Δv?
11. Suppose a radar views a target moving away from the radar at 50 m/s. The radiofrequency is 2 GHz. If the radar PRF is 2 kHz, what is the change in the echo phase shift from one pulse to the next? How many wavelengths does the target travel between two pulses?
12. Suppose the input to the coherent detector of Figure 8-12 is changed from a cosine function to a sine function. The argument of the sine function is the same as that of the cosine shown in the figure. How are the outputs of the detector changed? Which channel (upper or lower) will be the in-phase (I) output, and which the quadrature (Q) output?
13. An aircraft has a 4° azimuth 3 dB beamwidth. The RF is 10 GHz, and the antenna is steered to a squint angle, ψ, of 30°. If the aircraft flies at 150 m/s, what is the Doppler spread, B_{MLC}, of the clutter echoes induced by the aircraft motion?
14. Suppose the aircraft in problem 13 has a PRF of 10 kHz. Sketch a Doppler spectrum similar to that of Figure 8-21, but with noise and mainlobe clutter components only (no sidelobe clutter or moving targets). What range of Doppler shifts lies in the clutter region of the spectrum?

What range of Doppler shifts lies in the clear region of the spectrum? What percentage of the total spectrum width from $-PRF/2$ to $+PRF/2$ is in the clear region?

15. If the PRF in problem 14 is changed to 1 kHz, what percentage of the total spectrum width will lie in the clear region?

16. Equation (8.31) gives the Doppler bandwidth across the radar mainbeam due to motion of the radar platform for the case where the squint angle $\psi > \theta_3/2$ so that the mainbeam does not straddle the antenna boresight. Derive a formula for Doppler bandwidth for the case where $0 < \psi < \theta_3/2$ so that the mainbeam does straddle the boresight.

17. Consider a radar with a PRF of 5 kHz. What is the maximum unambiguous range, R_{ua}, of this radar, in km? If a target is located at a range of 50 miles, how many pulses will the radar have transmitted before the first echo from the target arrives? What will be the apparent range of the target in kilometers? (The apparent range is the range corresponding to the time delay from the most recent pulse transmission time to the arrival of the target echo from a previous pulse once steady state is achieved.)

18. Consider an airborne radar traveling straight, level, and forward at 200 mph at an altitude of 30,000 feet. The antenna is pointed at an azimuth angle of 0° and an elevation angle of -20°. Sketch the approximate unaliased range-velocity distribution of the ground clutter in a format similar to that of Figure 8-23b. The range axis of the sketch should cover 0 to 100 km, and the velocity axis should cover $\pm v_{max}$, where v_{max} is the maximum possible radial velocity in m/s that could be observed from scatterers in front of the radar. Indicate where the main lobe clutter is located on the sketch.

19. Suppose the radar in problem 18 has an RF of 10 GHz and a PRF of 3 kHz. What are the unambiguous range, R_{ua}, and unambiguous velocity, v_{ua}? Sketch the approximate aliased range-velocity distribution of the ground clutter in a format similar to that of Figure 8-25. The range axis of the sketch should cover 0 to R_{ua}, and the velocity axis should cover $\pm v_{ua}$. Indicate where the main lobe clutter is located on the sketch.